# Automatic Segmentation for Analysis of Murine Cardiac Ultrasound and Photoacoustic Image Data Using Deep Learning

Katherine Leyba, Hayley Chan, Olivia Loesch, Salomé Belec, Pierre Sicard, Craig Goergen

# Automatic Segmentation for Analysis of Murine Cardiac Ultrasound and Photoacoustic Image Data Using Deep Learning

Katherine A Leyba [1] , Hayley Chan [2] , Olivia Loesch [1] , Salomé Belec [3] , Pierre Sicard [3] , Craig J Goergen [4]

[1] Weldon School of Biomedical Engineering, Purdue University, West Lafayette, Indiana, USA.

[2] Indiana University School of Medicine, Indianapolis, Indiana, USA.

[3] PhyMedExp, IPAM/Biocampus, INSERM, CNRS, Université de Montpellier, Montpellier, France.

[4] Weldon School of Biomedical Engineering, Purdue University, West Lafayette, Indiana, USA. Electronic address: cgoergen@purdue.edu.

**Keywords:**

Cardiovascular disease; Deep learning; Oxygen saturation; Photoacoustic imaging; Strain; Ultrasound.

*** Corresponding author.**

**E-mail address:**

cgoergen@purdue.edu

(C.J. Goergen). 1

Pierre Sicard and Craig J. Goergen contributed equally to the paper.

# Abstract

**Objective:**

Although there are methods to identify regions of interest (ROIs) from echocardiographic images of myocardial tissue, they are often time-consuming and difficult to create when image quality is poor. Further, while myocardial strain from ultrasound (US) images can be estimated, US alone cannot obtain functional information, such as oxygen saturation ($sO_2$). Photoacoustic (PA) imaging, however, can be used to quantify $sO_2$ levels within tissue non-invasively.

**Methods:**

Here, we leverage deep learning methods to improve segmentation of the anterior wall of the left ventricle and apply both strain and oxygen saturation analysis via segmentation of murine US and PA images.

**Results:**

Data revealed that training on US/PA images using a U-Net deep neural network can be used to create reproducible ROIs of the anterior wall of the left ventricle in a murine image dataset. Accuracy and Dice score metrics were used to evaluate performance of the neural network on each image type. We report an accuracy of 97.3% and Dice score of 0.84 for ultrasound, 95.6% and 0.73 for photoacoustic, and 96.5% and 0.81 for combined ultrasound and photoacoustic images.

**Conclusion:**

Rapid segmentation via such methods can assist in quantification of strain and oxygenation.

# Introduction

Although methods exist to extract myocardial boundaries in ultrasound images semi automatically [1], these methods are often still time-consuming and dependent on image quality, as obtaining high quality ultrasound images depends on the skill of the technician [2]. Furthermore, standard ultrasound cannot obtain metabolic information from tissue, such as oxygenation, a key aspect of myocardial tissue health which is useful for determining the extent of ischemic injury after infarction [3]. Photoacoustic imaging is an emerging technology that combines both optics and acoustics, combining the contrast and specificity of optical imaging with the penetration depth of ultrasound [4]. Applying segmentation methods to dual-modality ultrasound and photoacoustic cardiac image data opens the possibility of quickly and accurately quantifying large image data sets, potentially reducing intra-user variability. Additionally, these segmentations can be used for evaluating cardiac tissue health via metrics such as strain and oxygenation. For example, Mukaddim et al.[5] and Liu et al.[6] demonstrated that estimation of oxygen saturation via optical imaging can be used to diagnose myocardial ischemia in real time.

Here, we report the implementation of a convolutional deep neural network, UN et an architecture that has been used to train on limited biomedical image data sets with impactful results [7−9], and use it to delineate regions of the myocardium in preclinical ultrasound and photoacoustic data sets with great efficiency compared to manual segmentation alone.

Results show that the segmentation algorithm works best on ultrasound images followed by the combined ultrasound and photoacoustic images and photoacoustic images alone. From the automatic segmentations generated by this algorithm, we estimate radial strain and oxygenation in the anterior myocardium of the left ventricle from animals with and without ischemic injury.

# Materials and methods

### Dataset

Murine data were acquired on a Vevo LAZR-X system (FUJIFILM Visual Sonics) using a linear array 5−30 MHz frequency (MX250) transducer and 750nm/850nm excitation wavelengths to obtain oxy-and deoxyhemoglobin information from each mouse throughout one cardiac cycle. The data set consists of 759(645 × 555 pixels) long-axis B-mode electrocardiogram-gated kilohertz visualization (EKV) ultrasound (US) and photoacoustic (PA) images, which can be combined into overlayed ultrasound and photoacoustic (USPA) images from 27 three-month-old male BALB/cJRj mice. Of the 27 mice, 17 were sham and 10 underwent a left coronary artery permanent ligation procedure as described previously [3], with images acquired 7d after surgery. From the data set, a trained sonographer created 759 manually segmented binary masks of the anterior portion of the left ventricle which served as the ROIs. Both the images and ROIs were split into 80% training (21 mice, 606 images) and 20% validation sets (6 mice, 153 images). Images in the training set were from14 sham mice and 7 myocardial infarction (MI) mice while images in the validation set were from 3 sham mice and 3 myocardial infarction (MI) mice. The authors confirm that Institutional Animal Care and Use Committee approval was obtained for the research procedures. Region of interest generation

Binary masks of the ROIs were generated manually on MATLAB (Natick, MA, USA) using the draw polygon function on the ultrasound images in which the ventral part of the myocardium was identified and isolated along the anterior wall of the left ventricle from base to apex.

**Implementation details**

Ultrasound, photoacoustic, and combined ultrasound/photoacoustic images along with the generated ROIs were scaled to 325×275 pixels to prevent heavy computational load and served as input to the deep neural network. The neural network was trained on a computer with an NVIDIAT500GPU (4GB memory) in PyCharm using the PyTorch frame-work and UN et deep neural network architecture. First, within the same algorithm, the neural network was trained on the EKV ultrasound image training set with manually generated binary masks and subsequently tested on the EKV ultrasound image validation set to generate predicted ROIs for15 epochs.

The EKV ultrasound images were then sharpened by using the insharpen function in MATLAB as a preprocessing step before feeding into the neural network again. We varied the strength of the sharpening effect with sharpening strength (s) set to 2, 3, and 4 (Fig.1). Wet hen compared the U-Net-Generated predicted ultrasound ROIs from the validation set to the ultrasound ROIs generated from manual segmentation, both with and without sharpening. Training with the U-Net deep neural network on the photoacoustic and combined ultrasound/photoacoustic images with and without sharpening was also accomplished using the same masks generated from the ultrasound set to generate predicted masks for both image types. Since sharpening did not improve training on the PA and USPA data, only results from training on the unsharpened PA and USPA images are reported. Accuracy (th e number of correct predictions over the total number of predictions) and Dice score (measuring segmentation overlap ranging from 0 to 1 [9]) metrics were used to evaluate algorithm performance of the US (sharpened), PA (unsharpened), and USPA (unsharpened) data.

**Cross validation**

Cross validation on our data set was performed using a combination of the k-fold and leave-one out methods on a subsample of the dataset [10]. This subsample consisted of 400 manually segmented binary masks of the anterior portion of the left ventricle which served as the manual ROIs. Both the images and ROIs were split into 77% training (9 mice,309 images) and 23% validation sets (3 mice, 91 images). Because of an imbalance in the number of mages within each sample, we used a more stratified approach in which data was partitioned so that at least one sample (data from one animal) was swapped in the test set while maintaining the total test set size to 21%−23% of the dataset form = 3 samples/mice. The deep neural network was then trained and tested with these various combinations of partitions in the test set to obtain a report of accuracy and Dice

The deep neural network was then trained and tested with these various combinations of partitions in the test set to obtain a report of accuracy and Dice scores. From these results, the dataset with the highest accuracy and Dice score was used to calculates train and sO2% within the manual and predicted ROIs.

**Strain calculation**

We calculated Green Lagrangian radial strain (Err) for the validation set for n = 6 mice (3 sham, 3MI) in MATLAB by measuring the thickness at the apical (t1), mid (t2, t3), and basal (t4) regions between the endocardium and epicardium of the manually segmented and predicted ROIs at end diastole and peak systole (Fig.3A), using the equation: where $r_{PS}$ is the radial thickness at peak systole and $r_{ED}$ is the radial thickness at end diastole. The difference between the manually segmented and predicted radial strain was also calculated.

$$e_{rr} = 0.5\left(\left(\frac{r_{PS}}{r_{ED}}\right)^2 - 1\right)$$

**Oxygen saturation calculation**

We calculated mean myocardial tissue oxygen saturation (sO2) within the regions segmented manually and automatically (predicted) on the photoacoustic images through a custom MATLAB script in which each RGB pixel value was mapped to arrange of 0 to 100 through implementation of a look up table. We then averaged the mapped values to obtain the mean tissues O2 within each segmentation.

**Statistical analysis**

An ANOVA multiple comparisons test with Tukey correction was used to compare radial strain and means O2% between the manual and predicted segmentations for all sham and MI mice in the test set. Levels of significance for the ANOVA multiple comparisons test are shown as $p<0.01$**, $p<0.001$***, $p<0.0001$****, and for no significance as $p>0.05$(ns). We used unpaired-t-tests to investigate differences between calculated radial strain and means O2 from the manual and predicted ROIs for the sham and MI mice combined. The threshold for significant difference for the t-tests and ANOVA multiple comparisons test was set top <0.05.

# Results

The results of our study show that our predicted ROIs matched up well with manually segmented ROIs, especially with sharpened ultra-sound data. The green contours represent the outline of the manual ROIs while the yellow contours represent the outline of the predicted ROIs, or ROIs that were generated as predicted by the deep neural network. Comparison between running th neural network before and after applying sharpening to the EKVB-mode ultrasound images is shown in Figure1, in which training on US images with sharpening strengths=3 produced the best accuracy and Dice score (Table1). The accuracy and Dice score

before sharpening on the EKVB-mode images was 97.35% and 0.783. After applying sharpening, the accuracy and Dice score post-training were improved, as shown in Table1.

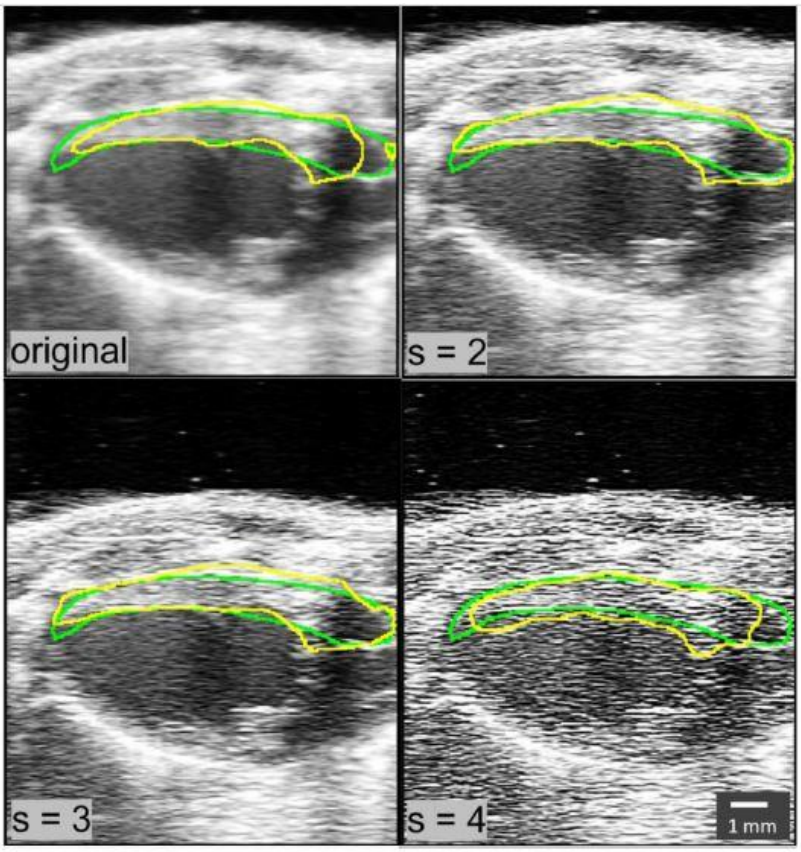


**Figure 1.** Enhancement of ultrasound images with local contrast adjusted via sharpening. The green contours indicate the manual ROIs while the yellow indicate the predicted ROIs. Original EKV B-mode image of murine cardiac left ventricle with various sharpening strengths (s = 2, s = 3, and s = 4) applied. A sharpening strength of s = 3 produced best results during training as defined by highest Dice score.

Results from running cross-validation are shown in Table 2 while accuracy and Dice score values from running the neural network algorithm on each dataset (US, PA, and USPA) are reported in Table 3.

**Table 1**
Comparison of neural network segmentation performance on ultrasound images of the cardiac left ventricle after applying contrast enhancement at various strength levels (s)

| Sharpening strength | Accuracy | Dice score |
|---|---|---|
| Original | 97.4% | 0.78 |
| s = 2 | 96.9% | 0.78 |
| s = 3 | 97.4% | 0.81 |
| s = 4 | 96.6% | 0.73 |

A comparison of some of the manually segmented and predicted ROIs on each dataset type is shown in Figure 2. The radial strain ratio (Fig.3) values for the manual and predicted ROIs in the validation set are shown in Supplemental Table1 while the difference between sham and MI mice radial strain (Fig.3B) and sO2 (Fig.4B ) are shown. Scatter and Bland-Altman plots showing the differenced average of the radial strain are shown in Figure 3 (C,D), respectively.

Mean tissues O2% values extracted from the manual and predicted ROIs in the validation PA images are shown in Figure 4 (A, B) for both sham and MI animals. Figure 4C showsthemeansO2% values of all 153 PA images in the validation set within manual and predicted ROIs while a Bland Altman plot showing the difference and aver-age of the means O2% values is shown in Figure 4D. Furthermore, segmentation with the U-Net took approximately 0.1−0.2 s/image compared to 45s/image manual segmentation, an over 200-fold improvement.

**Table 2**
Cross-validation shows that the neural network performs better on US and USPA images compared to PA images alone

| Image type | Accuracy | Dice score |
|---|---|---|
| US | 96.2% | 0.68 |
| PA | 95.6% | 0.66 |
| USPA | 96.2% | 0.68 |

Average accuracy and Dice scores reported on the ultrasound (US), photoacoustic (PA), and overlayed ultrasound and photoacoustic (USPA) datasets after running the neural network on 12 different combinations of training and validation sets for each image type from a 400-image subsample set.

**Table 3**
Comparison of neural network segmentation performance on ultrasound (US), photoacoustic (PA), and overlayed ultrasound and photoacoustic (USPA) images (759 per image type) of the cardiac left ventricle

| Image type | Accuracy | Dice score |
|---|---|---|
| US | 97.3% | 0.84 |
| PA | 95.6% | 0.73 |
| USPA | 96.7% | 0.81 |

# Discussion

In this study, we have proposed a method to automatically segment the anterior portion of the cardiac left ventricle in ultrasound, photoacoustic, and combined ultrasound/photoacoustic data to help streamline the process of evaluating cardiac tissue health metrics. The average accuracy and Dice scores from applying cross-validation were higher for the US and USPA data compared to the PA data, suggesting that U-Net performs better on US image data compared to PA alone. Furthermore, we demonstrate the utility of the automatic segmentations to obtain physiological parameters including cardiac radial strain and oxy- gen saturation, both of which can be useful for evaluating tissue health. For example, evaluation of cardiac tissue in an infarcted heart versus a healthy heart from these segmentations reveals reduced strain and oxygen saturation near the apex downstream of the coronary artery occlusion.

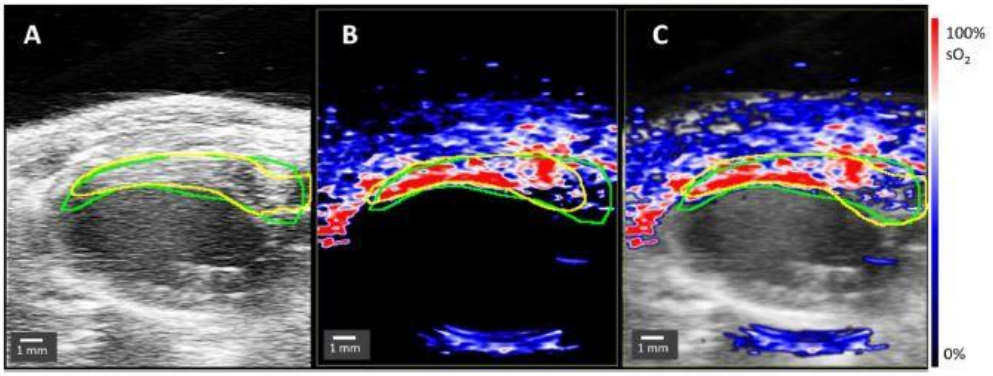


**Figure 2.** Predicted segmentations matched best with manual segmentations on datasets with ultrasound images. Examples of neural network segmentation performance on (A) ultrasound (US), (B) photoacoustic (PA), and (C) overlayed ultrasound and photoacoustic (USPA) images of the anterior wall of a murine left ventricle. Manually segmented ROIs (green) and predicted ROIs (yellow) align closely.

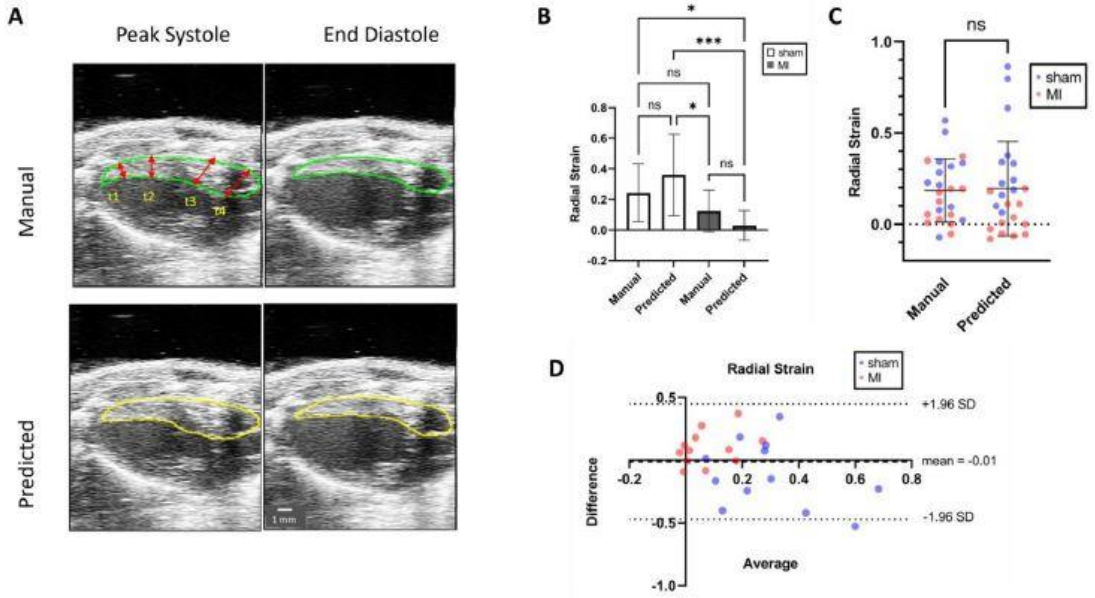


**Figure 3.** Manual and predicted segmentations reveal lower radial strain in infarcted myocardium compared to sham controls. (A) Example of where radial thickness measurements were taken to calculate radial strain from manual (green) and predicted ROIs (yellow) at end diastole and peak systole for a sham mouse in the validation set, (B) average radial strain comparison from manual and predicted segmentations between sham (n = 3) and MI (n = 3) mice within validation set, (C) scatter plot of mean ± SD radial strain values from manual and predicted ROIs, and (D) Bland-Altman plot of radial strain difference and average and standard deviation between manual and predicted ROIs from values reported in Supplemental Table 1. Average radial strain was calculated per mouse in validation set (n = 6) at four different locations (t1, t2, t3, and t4) along the myocardium and is expressed as a ratio. The levels of significance for (B) and (C) are $p < 0.05$*, $p < 0.001$***, and $p$ = ns (no significance).

To further improve segmentation accuracy and speed, the use of a computer cluster could be employed. Other potential improvements could include pre-and post-processing methods such as data augmentation and artifact removal, regularization methods such as dropout, applying transfer learning (i.e., training on US data first, then apply transfer learning to the PA data or vice versa), or further expanding the data set size. For example, by employing regularization, the deep neural network is better equipped to make predictions with higher accuracy and Dice score on new inputs or with data it has never seen before [11]. This can help in the problem of overfitting where the deep learning model can generalize to new data instead of memorizing the data it is trained on. The implications of this study are wide spread—not only is this deep learning method capable of improving segmentation and analysis time of murine cardiac image datasets but it has the potential to eventually be applied toward larger and more clinically relevant data in which physicians must make time-sensitive decisions.

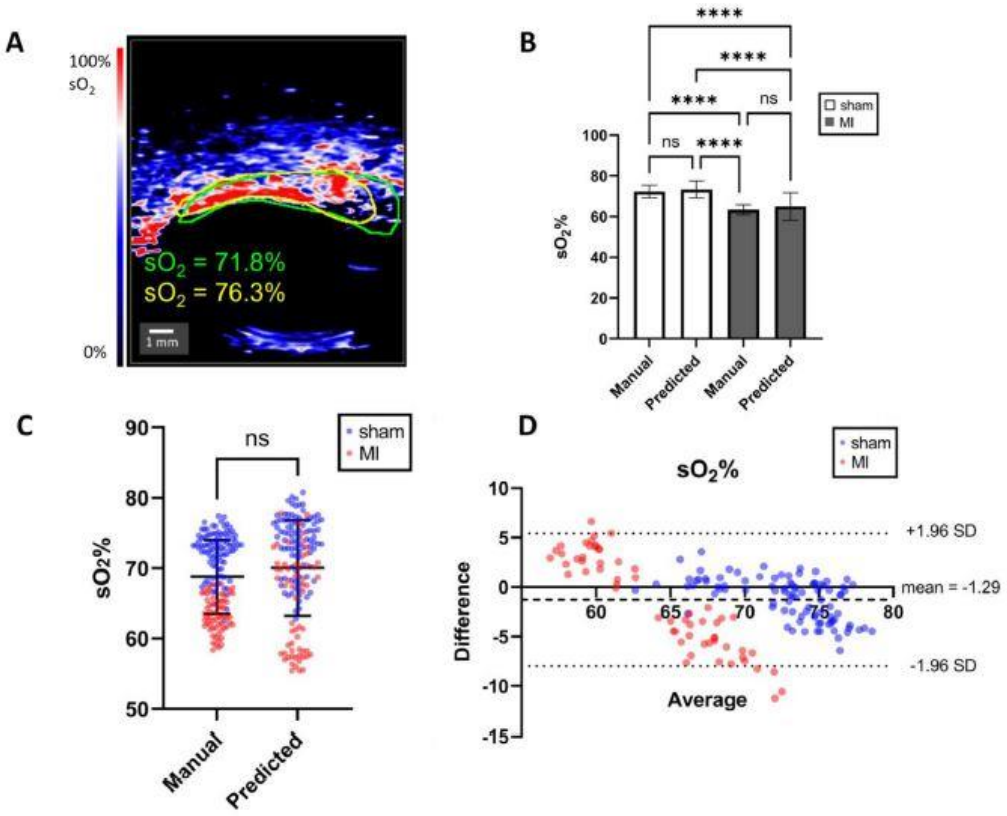


**Figure 4.** Manual (green) and predicted (yellow) ROIs reveal lower oxygen saturation in infarcted myocardium compared to sham controls. (A) Comparison of mean oxygen saturation ($sO_2$) in anterior myocardium of sham mouse from validation set between manual (green) and predicted (yellow) segmentation in a photoacoustic image, (B) average oxygen saturation comparison from manual and predicted segmentations between sham (n = 3) and MI (n = 3) mice within validation set, (C) scatter plot of mean oxygen saturation ($sO_2$) from manual and predicted segmentations in validation set with results expressed as mean ± SD, and (D) Bland-Altman plot showing difference vs. average of mean $sO_2$% extracted from manual and predicted segmentations in validation set. The levels of significance for (B) and (C) are $p <$ 0.0001****, and $p$ = ns (no significance).

# Conclusion

Here, we show how deep learning can be used to segment myocardium from both preclinical ultrasound and photoacoustic murine image data. Our results were comparable to manually segmented data with a reduction in segmentation time by over 200-fold. Overall, this study lays the ground work for improving analysis of cardiac images to accurately and efficiently monitor cardiac health.

## Conflict of interest

Dr.CraigJ.GoergenisapaidconsultantofFUJIFILMVisualSonicsInc.FUJIFILMVisualSonicshad noroleinstudydesign,execution,orwriting.Allotherauthorsdeclarenoconflictsofinterest.DataavailabilityThedatathatsupportthefindingsofthisstudyareopenlyavailableinthePurdueUniversityResearchRepositoryathttp://doi.org/10.4231/9C8X-H052.

## Acknowledgments

We would like to acknowledge the PhyMedExp's animal housing staff and the Imagerie du Petit Animal de Montpellier (IPAM, Biocampus) for ultrasound and photoacoustic images (LRQA Iso9001; France Life Imaging (grantANR-11-INBS-0006); IBISA; Leducq Foundation (RETP),I-Site Muse). This work was supported by the National Science Foundation for support under the Graduate Research Fellowship Program (GRFP) under grant number DGE-1842166; under the Fulbright United Scholar Program; under the Montpellier

Advanced Knowledge Institute on Transitions (MAK'IT) Program of the Université de Montpellier; and under the Thomas Jefferson Fund from the French-American Cultural Exchange (FACE) Foundation. This work involved laboratory animals.

# References

[1] Kim T, Hedayat M,Vaitkus VV, Belohlavek M, Krishnamurthy V ,Borazjani I. Automatic segmentation of the left ventricle in echocardiographic images using convolutional neural networks.QuantImagingMedSurg2021;11(5):1763 81.

[2] Stasi G, Ruoti EM. A critical evaluation in the delivery of the ultrasound practice: the point of view of the radiologist.ItalJMed2015;9(1):5.

[3] David H, Ughetto A, Gaudard P, Plawecki M, Paiyabhroma N, Zub E, et al. Experimental myocardial infarction elicits time dependent patterns of vascular hypoxia in peripheral organs and in th ebrain.FrontCardiovascMed2021;7:615507.

[4]BeardP. Biomedical photoacoustic imaging.InterfaceFocus2011;1(4):602–31.

[5]LiuY,HanleyT,ChenH,LongS,GambhirS,ChengZ,etal.Non-invasivephoto acoustic imaging of in vivo mice with erythrocyte derived optical nanoparticles to detect CAD/MI.SciRep2020;10:5983.

[6] Mukaddim RA, Rodgers A, Hacker T, Heinmiller A, Varghese T. Real-timeinvivopho-toacousticimagingintheassessmentofmyocardialdynamicsinmurinemodelofmyocardialischemi a.UltrasoundMedBiol2018;44(10):P2155–64.

[7] Ronneberger O, Fischer P, Brox T U-Net : Convolutional networks for biomedical image segmentation.2015;Accessed25Aug,2-023,https://arxiv.org/abs/1505.04597

[8] Müller D, Soto-Rey I, Kramer F. Robust chest CT image segmentation of COVID-19lung infection based on limited data.InfMedUnlocked2021;25:100681.

[9]BardisM,HoushyarR,ChantadulyC,UshinskyA,GlavisBloomJ,ShaverM,ChowD,UchioE,Ch angP.Deeplearning with limited data: organ segmentation performance byU-net.Electronics2020;9:1199.

[10] Wong TT. Performance evaluation of classification algorithms by k-fold and leave-one-outcross validation.PatternRecognit2015;48(9):2839–46.

[11]GoodfellowI,BengioY,CourvilleA.Deeplearning.MITPress;2016http://www.deeplearning book.org.